0026-895X/99/010214-12$3.00/0

MOLECULAR PHARMACOLOGY, **56:**214–225 (1999).

Activation Mechanism of Human Oxytocin Receptor: A Combined Study of Experimental and Computer-Simulated Mutagenesis

FRANCESCA FANELLI, PASCALINE BARBIER, DEBORAH ZANCHETTA, PIER G. DE BENEDETTI, and BICE CHINI

Department of Chemistry, University of Modena, Modena, Italy (F.F., P.G.DeB.); Consiglio Nazionale delle Richerche Cellular and Molecular Pharmacology Center, Department of Pharmacology, University of Milan, Milan, Italy (P.B., D.Z., B.C.)

Received August 5, 1998; accepted April 20, 1998

This paper is available online at http://www.molpharm.org

ABSTRACT

The aim of this study was to investigate the molecular changes associated with the transition of the human oxytocin receptor from its inactive to its active states. Mutation of the conserved arginine of the glutamate/aspartate-arginine-tyrosine motif located in the second intracellular domain gave rise to the first known constitutively active oxytocin receptor (R137A), whereas mutation of the aspartic acid located in the second transmembrane domain led to an inactive receptor (D85A). The structural features of the constitutively active and inactive receptor mutants were compared with those of the wild type in its free and agonist-bound states. The results suggest that, although differently triggered, the activation process induced by the agonist and the activating mutation are characterized by the opening of a solvent exposed site formed by the 2nd intracellular loop, the cytosolic extension of helix 5, and the 3rd intracellular loop; on the contrary, the D85A mutation prevents oxytocin from triggering the opening of a cytosolic site. On the basis of these findings, we hypothesize that this cytosolic crevice plays an important role in G protein recognition. Finally, comparative analysis of the free- and agonist-bound forms of the wild-type oxytocin receptor and α_{1B} adrenergic receptor suggests that the highly conserved polar amino acids and the seven helices play similar mechanistic roles in the different G protein-coupled receptors.

Receptors of the rhodopsin family use G proteins to transduce signals across the cell membrane. All of these receptors share the presence of seven hydrophobic regions, which are believed to form a bundle of α-helical transmembrane domains connected by intracellular and extracellular loops. Mutational analysis has revealed that the extracellular regions and transmembrane domains contribute toward the formation of the ligand binding site, whereas the intracellular loops appear to mediate G protein coupling (Wess, 1997). Despite the fact that recent crystallographic studies of G proteins have begun to show how they might work (Coleman and Sprang, 1996), a consistent description in terms of the structure and dynamics of the mechanisms of receptor activation and receptor-catalyzed nucleotide exchange still remains a daunting task.

The discovery that mutations in the third intracellular loop of different adrenergic receptors (ARs) can greatly increase their constitutive (agonist-independent) activity led to the hypothesis that G protein-coupled receptors (GPCRs) can exist in equilibrium between interconvertible inactive (R) and active (R*) allosteric states (Cotecchia et al., 1990; Samama et al., 1993). Recent studies on rhodopsin showed that the light-activated conformational changes appear to involve rigid body motions of helix F relative to helix C (helices C and F in rhodopsin correspond to helices 3 and 6 in the other homologous GPCRs) (Farrens et al., 1996) and experiments on β_2-AR showed that agonist-induced receptor activation involves movements of helices 3 and 6 (Gether et al., 1997). These results emphasize the need to develop a dynamic description of GPCR proteins to elucidate the structural changes associated with functionally different states.

The pattern of the microscopic configurations that predominate in each functional form of the α_{1B}-AR have very recently been investigated (Scheer et al., 1996, 1997; Fanelli et al., 1998). These studies suggested that certain highly conserved polar amino acids located in the seven-helix bundle may drive the motion of the helices that culminates into the rearrangement of the cytosolic domains involved in receptor/G protein recognition. In particular, the model showed

This work was supported by grants from Consiglio Nazionale delle Richerche (CNR) and Associazione Italiana Ricerca sul Cancro to B.C.

ABBREVIATIONS: AR, adrenergic receptor; WT, wild-type; OTR, oxytocin receptor; OT, oxytocin; G protein, guanine nucleotide binding protein; GPCR, G protein-coupled receptor; R, inactive receptor conformation; R*, active receptor conformation; E/DRY, glutamate/aspartate-arginine-tyrosine; AVP, arginine-vasopressin; OTA, d(CH_2)$_5$[Tyr(Me)$_2$,Thr4,Tyr-9-NH_2]-OVT; GTPγS, guanosine 5′-3-*O*-(thio)triphosphate; InsP, inositol phosphate; EGFP, enhanced green fluorescent protein; MD, molecular dynamics; t, transmembrane; e, extracellular; i, intracellular.

that the aspartate and arginine residues of the glutamate/aspartate-arginine-tyrosine (E/DRY) sequence, as well as of the N63, D91, N344, and Y348 residues that form a conserved polar pocket near the cytosol, play a fundamental role in regulating receptor isomerization into functionally different states. Although it is known that the E/DRY residues are conserved in almost all GPCRs and are essential to the coupling process in many different receptors, it is still not clear whether and how this sequence plays a general role in controlling the transition from inactive to active states.

The main aim of this study was to investigate whether the control by the E/DRY region of the transition from R to R*, which has been proposed to occur in the α_{1B}-AR, is maintained in the oxytocin receptor (OTR), a peptidergic receptor belonging to the oxytocin (OT)/arginine-vasopressin (AVP) receptor family, which also includes the V_{1a}, V_{1b}, and V_2 subtypes. A number of functional and structural aspects of these receptors have recently been elucidated at the molecular level by means of chimeric receptors (Postina et al., 1996) and a combination of molecular modeling and site-directed mutagenesis (Chini et al., 1995; Mouillac et al., 1995; Chini et al., 1996); in particular, several receptor residues and regions have been shown to be involved in determining the selective affinities and efficacies of different peptides to the different receptor subtypes; the receptor regions that specifically interact with G proteins (Liu and Wess, 1996) have also been identified. Even though a constitutively active V_2 vasopressin receptor has been recently described (Morin et al., 1998), the structural and dynamic changes associated with the agonist-independent and agonist-induced transition from inactive to active states have never been studied in this receptor family.

To investigate the R/R* transition in the human OTR in this study, the highly conserved amino acids N57 (helix 1), D85 (helix 2), D136 (helix 3), and R137 (helix 3) (the last two of which belong to the highly conserved E/DRY sequence) were subjected to experimental and computer-simulated mutagenesis. A comparative analysis of the molecular dynamics (MD) trajectories of the wild-type (WT) OTR as well as of the R137A and D85A mutants was performed. This approach led to the discovery of the activating mutation R137A and the inactivating mutation D85A. To compare constitutive and agonist-induced activation, MD of the OT-bound forms of the WT OTR, as well as of the D85A mutant were also simulated. Finally, a comparative analysis of the active and the inactive states of OTR with those of the α_{1B}-AR were made to investigate whether the members of the rhodopsin family of GPCRs might have similar activation mechanisms.

Materials and Methods

Peptides and Chemicals. Synthetic OT was obtained from Bachem Switzerland. The specific OTR antagonist OTA was synthesized in the laboratory of Dr. M. Manning and iodinated in the laboratory of C. Barberis as described previously (Elands et al., 1987). Guanosine 5′-3-*O*-(thio)triphosphate (GTPγS) and BSA were purchased from Sigma Chemical Co. (St. Louis, MO). [^{3}H]OT (35–45 Ci/mmol), [^{3}H]AVP (35–45 Ci/mmol), and myo-[2-^{3}H]inositol (10–20 Ci/mmol) were from Dupont-NEN (Boston, MA).

Construct Preparation. The human OTR cDNA, a generous gift of Dr. T. Kimura was subcloned into an M13 vector (M13 mp18) and the mutants were constructed by means of oligonucleotide-directed mutagenesis (Sculptor Kit; Amersham Corp., Arlington Heights, IL). WT and mutant cDNAs were then inserted into an eukaryotic expression vector under the control of the cytomegalovirus promoter (pRK5). For checking transfection efficiency by means of fluorescence-activated cell sorting analysis (FACS) analysis, WT and mutant cDNAs were subcloned into the internal ribosome entry site enhanced green fluorescent protein (pIRES-EGFP) vector (Clontech, Palo Alto, CA).

Cell Transfection. The WT and mutant receptors were transiently transfected into COS7 cells (American Type Culture Collection, Rockville, MD) by electroporation. The COS7 cells were grown in Dulbecco's modified Eagl's medium (Gibco BRL, Gaithersburg, MD) supplemented with 10% fetal calf serum (Sigma), 100 IU/ml penicillin, and streptomycin (Gibco BRL), in 5% CO_2 in air, at 37°C. Electroporation (280V, 960 μF, Bio-Rad gene pulser electroporator; Bio-Rad Labs., Hercules, CA) was performed in a total volume of 300 μl with 10^7 cells in electroporation buffer (50 mM $KHPO_4$, 20 mM CH_3COOK, and 20 mM KOH) and various amounts of plasmid DNA (vector with a subcloned insert) and carrier DNA (vector without insert) to reach a total amount of 20 μg of DNA/transfection. After electroporation, the cells were split into 6-well clusters [for the determination of inositol phosphate (InsP) accumulation], 24-well clusters (for intact cell binding assays), 150-mm petri dishes (for membrane preparation) or 100-mm petri dishes for FACS analysis.

Receptor Binding Assay. To determine cell surface binding, the cells were subcultured into 24-well plates at a density of 4×10^5 cells/well; 72 h after transfection, the cells were washed twice with binding buffer (146 mM NaCl, 4.2 mM KCl, 0.5 mM $MgCl_2$, 1.0 mM $CaCl_2$, 10 mM HEPES base, 1% glucose, 0.018% L-tyrosine, and 1% BSA, pH 7.4) and placed on ice. Increasing concentrations of [^{3}H]OT were added to the wells with or without 10^{-6} unlabeled OT in a final volume of 200 μl. After incubation for 2 h at 4°C, the cells were washed three times with cold binding buffer to remove the unbound radioactivity and then solubilized with 0.5 N NaOH. The samples were transferred into scintillation vials and counted using a beta counter after the addition of 3.5 ml of scintillation cocktail (Ultima Gold; Packard, Meridan, CT). To prepare the membranes, transfected COS7 cells were homogenized in a glass potter, washed twice, and resuspended in the binding buffer (50 mM Tris HCl, 5 mM MgCl, pH 7.4). Homogenates were used immediately or frozen under liquid nitrogen and stored at −70°C. For saturation experiments performed in presence or absence of GTPγS only freshly prepared homogenates were used. When [^{125}I]OTA was used, 1 to 5 μg of membrane proteins were incubated for 60 min at 30°C; when [^{3}H]OT and [^{3}H]AVP were used, incubation lasted 30 min in the presence of 5 to 10 μg of membrane proteins. Nonspecific binding was determined in the presence of a 250- to 1000-fold excess of unlabeled analogs. Bound and free radioactivity were separated by filtration over Whatman GF/C filters presoaked in 10 mg/ml BSA. Binding isotherms were analyzed with the iterative curve-fitting program LIGAND (Munson and Rodbard; 1980).

InsP Determination. InsP accumulation was determined as previously described (Mouillac et al., 1995). Briefly, transfected cells were grown on six-well dishes for 48 h. The cells were then labeled for 24 h with myo-[2-^{3}H]inositol at a final concentration of 2 μCi/ml in a serum-free, inositol-free medium (Gibco BRL). The cells were washed twice in Krebs buffer (146 mM NaCl, 4.2 mM KCl, 0.5 mM $MgCl_2$ 1.0 mM $CaCl_2$ 10 mM HEPES base, and 1% glucose, pH 7.4) and preincubated at 37°C in the same buffer supplemented with 10 mM LiCl. After incubation for 20 min in the absence (basal) or presence of increasing peptide concentrations (from 10^{-15} to 10^{-5}), the reaction was stopped with percloric acid, and the InsPs were extracted and separated using a strong anionic exchange column (Dowex AG1 × 8, formate form, 200–400 mesh; Bio-Rad). At each concentration, a fraction containing inositol monophosphates, bisphosphates, and trisphosphates was collected and its radioactivity determined by means of scintillation counting. This fraction is referred to as total InsP and expressed as disintegrations per minute per well. The data were analyzed by means of nonlinear regression

using a sigmoidal dose-response equation (Prism, GraphPad, San Diego, CA).

FACS Analysis. For flow cytometry, cells were scraped and resuspended in PBS^{-}/2.0 mM EDTA at a concentration of 1 to 2 $\times$ 10^6 cells/ml. Flow cytometry analysis was performed with a FACScan (Cell Quest software; Becton Dickinson, Lincoln Park, NJ). Cells were gated for size and side scatter to exclude dead cells and debris.

Three-Dimensional Model Building of OTR and OT/OTR Complex. Figure 1 shows the transmembrane (t), extracellular (e), and intracellular (i) domains included in the OTR model, together with the secondary structures assigned to the input receptor model. The lengths of the seven helices were chosen on the basis of multiple sequence alignments and predictions of the topology of the transmembrane segments (Rost et al., 1996). Helices 3, 5, 6, and 7 were extended into the cytosol on the basis of several lines of evidence, including NMR and circular dichroism experiments on synthetic peptides derived from the third and fourth intracellular loops of rhodopsin, β_2-AR, and angiotensin II receptors (Jung et al., 1995, 1996; Yeagle et al., 1997; Franzoni et al., 1997). The extracellular ends of the helices were also slightly prolonged.

In the input arrangement, the seven helices were packed using the recently published backbone coordinates of the upgraded version of the α_{1B}-AR model as an initial template (Fanelli et al., 1998). The helices were translated and rotated to relieve steric conflicts and improve the helix-helix packing according to the tilt of the seven helices derived from the three-dimensional map of frog rhodopsin (Unger et al., 1997).

The intracellular and extracellular loops (excluding i3) were built following the same procedure as that previously described for the α_{1B}-AR. The 242 to 270 stretch of amino acids belonging to i3 was built by restraint-based comparative modeling (Sali and Blundell, 1993), using the NMR structure of the third intracellular loop of the parathyroid hormone receptor as the initial template (Pellegrini et al., 1996). A disulphide bridge was allowed to form between C112 and C187, in accordance with experimental evidence.

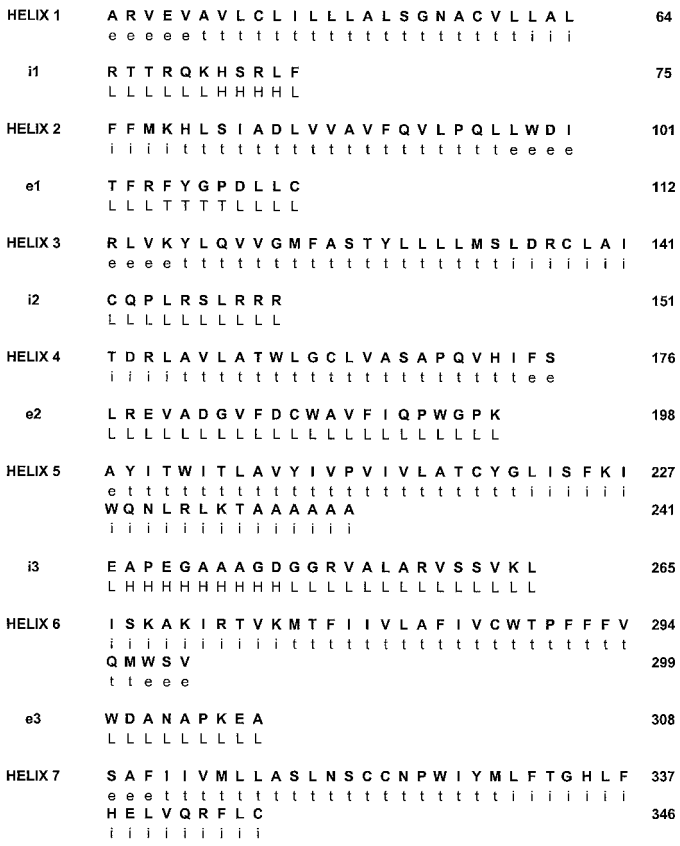

Fig. 1. Amino acids included in the theoretical model of the human OTR. Model includes the seven helices, the three extracellular loops (e1, e2, and e3), and the three intracellular loops (i1, i2, and i3). For the intracellular (i) and the extracellular (e) receptor domains, the secondary structure (H, helix; T, turns; L, loop) assigned in the input arrangement is indicated. For the helices, the predicted topology (e, extracellular; t, transmembrane; i, intracellular) is indicated.

Different input arrangements were built by performing translations and rotations of the helices and loops, as well as modifications of the side chain torsion angles. An input structure of the WT OTR was finally selected among the large number of tested arrangements; upon MD simulations, this structure produced an average arrangement showing the best agreement with the experimental data available on GPCRs together with high quality check scores.

The input structures of the mutant receptor forms were obtained by substituting the target residue in the selected WT input structure using the molecular graphics package QUANTA (release 96; Molecular Simulations Inc., Waltham, MA). The input structure of the OT-WT OTR complex was obtained by docking OT into the input structure of the WT OTR. The OT extracted from the crystal structure of the OT-neurophysin complex (Protein Data Bank code: 1npo) (Rose et al., 1996) was tested, as was that obtained from deamino OT (Protein Data Bank code: 1xy2) (Woods et al., 1986). The main orientation of the hormone was chosen following the suggestions of experimental results obtained using vasopressin receptors (Kojro et al., 1993; Chini et al., 1995) and experiments on vasopressin/OT chimeric receptors (Postina et al., 1996). These experiments indicated that the cyclic part of the hormone should interact with e2 and e3, whereas the linear C-terminal peptide should be oriented toward the N-terminal tail and e1. Different initial orientations of the hormone were tested, as were different initial conformations of its backbone C-terminal tripeptide and of the amino acid side chains involved in OT-OTR interactions. The OT-OTR complexes were submitted to energy minimization and MD simulation. Among the large number of OT-OTR complexes obtained, the model showing the best agreement with the experimental data mentioned above was selected for the comparative analysis. The input structure corresponding to this complex carries the OT extracted from the OT-neurophisin complex (Rose et al., 1996).

The input structure of the OT-D85A complex was obtained by mutating D85 in the selected input structure of the OT-bound WT OTR.

Computations. The minimizations and MD simulations were made using the CHARMM program (Brooks et al., 1983). Minimizations were carried out using 1500 steps of steepest descent followed by a conjugate gradient minimization, until the root mean square gradient was less than 0.001 kcal/mol. A distance-dependent dielectric term ($\epsilon = 4r$) and a 12 Å nonbonded cutoff distance were chosen. The "united atom approximation" was used for computational efficiency (Brooks et al., 1983). The minimized coordinates of the receptors and hormone-receptor complexes were then used as the starting point for a 150-ps MD run. The systems were heated to 300 K with a 5°C rise per 6000 steps by randomly assigning velocities from the Gaussian distribution. After heating, the system was allowed to equilibrate for 34 ps. Velocities were scaled by a single factor. The system was then subjected to 110 ps MD simulation at a constant temperature (300 K). The reported results were collected every 0.5 ps from the last 100 ps trajectory. The lengths of the bonds involving hydrogen atoms were constrained according to the SHAKE algorithm, allowing an integration time step of 0.001 ps. Newton's equations of motion were integrated using the Verlet algorithm. The α-helix conformation was preserved by using the nuclear Overhauser effect constraint with a scaling factor of 10. These constraints were applied between the backbone oxygen atom of residue i and the backbone nitrogen atom of residue i + 4, excluding prolines. Different combinations of distance constraints were tested.

Different prototropic forms of the WT OTR, involving the histidines in the seven-helix bundle as well as the highly conserved

aspartate of the E/DRY sequence (D136), were simulated. Because H173 (helix 4) and H335 (helix 7) should lie at a pH lower than 7.4 due to the closeness of phospholipids, and should therefore be suitable for protonation, the average minimized structure carrying all of the histidines but H173 and H335 in their neutral form were finally considered in the comparative analysis. This combination of charged states involving the histidines was associated with each of the two possible prototropic forms of D136: the deprotonated (anionic) and protonated (neutral) form. The receptor structure carrying D136 in its deprotonated form was finally considered for the comparative analysis. The comparative analysis was performed on the structures averaged over the last 100 ps of the equilibrated time period of each MD simulation and minimized.

The selected input structure and the computational conditions finally chosen produced average arrangements of the WT OTR, of the mutants, and of the OT-bound receptor forms consistent, especially for the active forms, with the structural features recently inferred from a wide analysis of the GPCR sequences (Baldwin et al., 1997).

The Protein Health utility implemented in QUANTA (release 96; Molecular Simulations Inc.) was used to check the quality of the models obtained.

Results

Expression of WT and mutant OTRs in COS7 cells. To investigate the role played by highly conserved residues in determining the active and inactive states of the human OTR, the N57A, D85A and D136A, D136Q, and R137A mutations were introduced into the WT OTR receptor by site-directed mutagenesis. The binding and coupling properties of all of the receptor mutants were assayed upon transient transfection in COS7 cells as described in *Materials and Methods*. The cells transfected with the N57A, D136A, and D136Q mutants did not show any specific binding when probed in saturation binding assays with labeled agonists ([^{3}H]OT and [^{3}H]AVP) or antagonists ([^{125}I]OTA); furthermore, they were completely unresponsive when assayed for InsP production upon stimulation with high doses of OT and AVP (10^{-5} M; data not shown). This indicates that these receptor mutants are either completely functionally inactive or that they are trapped inside the intracellular compartments due to folding, sorting, and/or recycling defects. On the contrary, the R137A and the D85A mutants were sorted to the plasma membrane, as indicated by binding analysis of intact cells; however, we had to increase the amount of specific DNA transfected (plasmid with a subcloned receptor cDNA) by a factor of 10 to achieve a level of expression similar to that of the WT. The total amount of DNA transfected (20 μg/electroporation) was maintained constant by decreasing the carrier DNA (plasmid without insert). Under these conditions, the B_{max} values for the WT and the R137A mutant, as measured by means of [^{3}H]OT saturation experiments with intact cells, were 426,300 ± 157,400 (n = 3) and 435,000 ± 50,140 (n = 3) sites/cell, respectively. The K_D values were also similar: 2.99 ± 0.41 nM (n = 3). and 5.42 ± 1.69 nM (n = 3), respectively. In the case of the D85A mutant, the level of expression was determined by means of [^{3}H]AVP homologous competition because no specific binding was detected when [^{3}H]OT was used in saturation and competition experiments. Our data indicate an expression of 298,600 ± 172,700 sites/cells (n = 2) and a very large decrease in AVP affinity (K_i = 1350 ± 826 nM; n = 2) in comparison with the WT receptor (K_i = 1.65 ± 0.49 nM; n = 2).

Coupling Properties of R137A (Constitutively Active) and D85A (Inactive) Mutants. To determine the coupling properties of the R137A and D85A mutants, the basal production of total InsP was measured in transiently transfected COS7 cells expressing similar levels of WT or mutant OTRs (0.4–0.5 pmol/mg of proteins). As shown in Fig. 2A, our data indicate that the R137A induced a significant increase in the basal production of total InsP; if the basal level of total InsP in mock-transfected cells is taken as 100%, this increase was estimated to be 145% (n = 5, p > .001). At this level of expression, there was no difference in the basal InsP production by the WT receptor and that by the mock-transfected cells. Furthermore, the maximum level of InsP production induced by treatment with 10^{-5} M OT was similar for the two receptors (3–5 times more than basal; Fig. 2B),

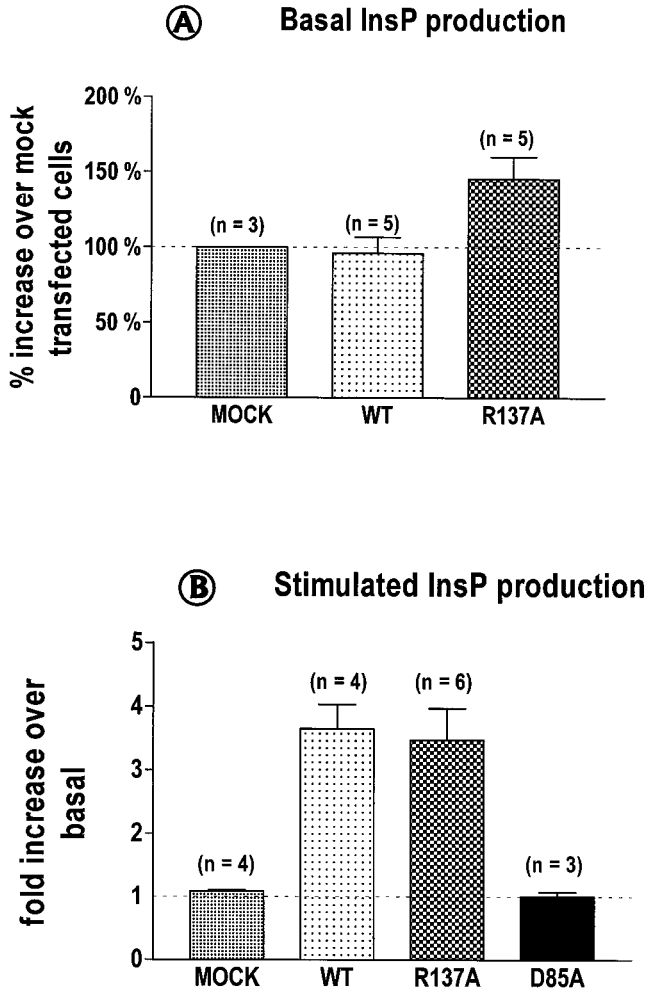

Fig. 2. Basal and stimulated activation of WT, R137A, and D85A OTR receptors. WT, R137A, and D85A receptors were transiently expressed in COS7 cells and their coupling to Gq/G11 was evaluated by measuring the accumulation of total InsP over a period of 15 min. A, basal InsP levels. Graph shows the mean values of five different experiments; in each experiment, performed in triplicate, the basal InsP production of the WT and R137A mutant was expressed as the percentage of increase over that of mock-transfected cells (taken as 100%). B, agonist-stimulated InsP levels. In these experiments, the maximum InsP production was measured by applying a high dose of OT (10^{-5} M). For each receptor, the basal level of InsP production was fixed to the value of 1 and the ratio between the maximum InsP production obtained with 10^{-5} M OT and basal InsP production was calculated. This ratio is shown on the ordinate axis as the fold increase over basal.

whereas no detectable increase in InsP production was observed in the D85A mutant under basal or stimulated conditions. Because the D85A mutant retained a measurable affinity for AVP, we also checked InsP production after treatment with 10^{-5} M AVP; once again, no detectable variation in InsP accumulation was detected (not shown). These data indicate that we obtained one constitutively active mutant (R137A) that is still responsive to OT, and one that is unable to stimulate phospholipase C and is functionally inactive (D85A).

To evaluate whether variations of transfection efficiency between the WT and the R137A mutant may have influenced our findings, we subcloned the WT OTR and the constitutively active R137A mutant into the multicloning site of the pIRES-EGFP vector (Clontech). This vector contains the IRES sequence of the encephalomyocarditis virus between the multicloning site and the EGFP; the IRES sequence permits the translation of two open reading frames from a single mRNA. The transfection of our constructs (WT-OTR-pIRES and R137A-pIRES) led to the coexpression of the receptor and EGFP in the same cells, thus allowing transient transfection efficiency to be evaluated by means of FACS analysis. In preliminary experiments, we investigated whether transfection efficiency varied when increasing amounts of pIRES-EGFP DNA were electroporated. As shown in Fig. 3A, for amounts of specific DNA ranging from 0.75 to 10 μg, transfection efficiency was between 17 and 37%; at lower DNA concentrations, transfection efficiency dropped (3% for 0.075 μg of transfected DNA). These data indicate that transfection efficiency remains fairly constant for quantities of specific DNA ranging from 0.75 to 10 μg and with carrier DNA added to reach 20 μg of DNA/electroporation. We then determined the amount of specific DNA needed to obtain a B_{max} of approximately 1 pmol of receptor/mg of protein (not shown). These amounts of DNA, 0.75 μg of WT-OTR-pIRES, and 7.5 μg R137A-pIRES, are approximately 10 times more than that used with our constructs in the pRK5 vector (0.09 and 0.9 μg for the WT and R137A, respectively); although both plasmids use a cytomegalovirus promoter, they have different enhancer, synthetic-splicing, and polyadenilation signals, and these differences may explain their different ability to drive heterologous protein expression. Figure 3, B and C, shows the results of one of two experiments in which we used flow cytometry to measured the percentage of cells transfected with WT-OTR-pIRES and R137A-pIRES. In these experiments, the transfection efficiencies were highly comparable (30 and 28% in the first experiment, 16 and 18% in the second) as were their B_{max} values (1.05 and 1.31 pmol/mg protein in the first experiment, 1.34 and 1.65 pmol/mg protein in the second). At this level of expression, the basal activity of the R137A and WT OTR had increased to 177% ($n = 2$) and 116% ($n = 2$) that of the mock-transfected cells. These data confirm that the R137A mutant is characterized by a basal activity higher than that of the wild-type receptor.

To better analyze the coupling properties of the R137A mutant, we drew the dose-response curves of total InsP accumulation upon agonist stimulation. As shown in Fig. 4A, R137A was able to stimulate phospholipase C in a dose-dependent manner with a calculated EC_{50} for OT of 57.4 ± 24.4 nM ($n = 3$); this value differs by approximately a factor 10 from that of the WT receptor expressed in the same cells (4.8 ± 0.8 nM; $n = 3$). Finally, the inverse agonist properties of the specific peptidic antagonist OTA were assayed in cells transfected with the R137A mutant. As shown in Fig. 4B, this analog had inverse agonist properties with a measured IC_{50} of 0.2415 pM ($n = 2$).

Finally, to correlate the basal InsP production with the

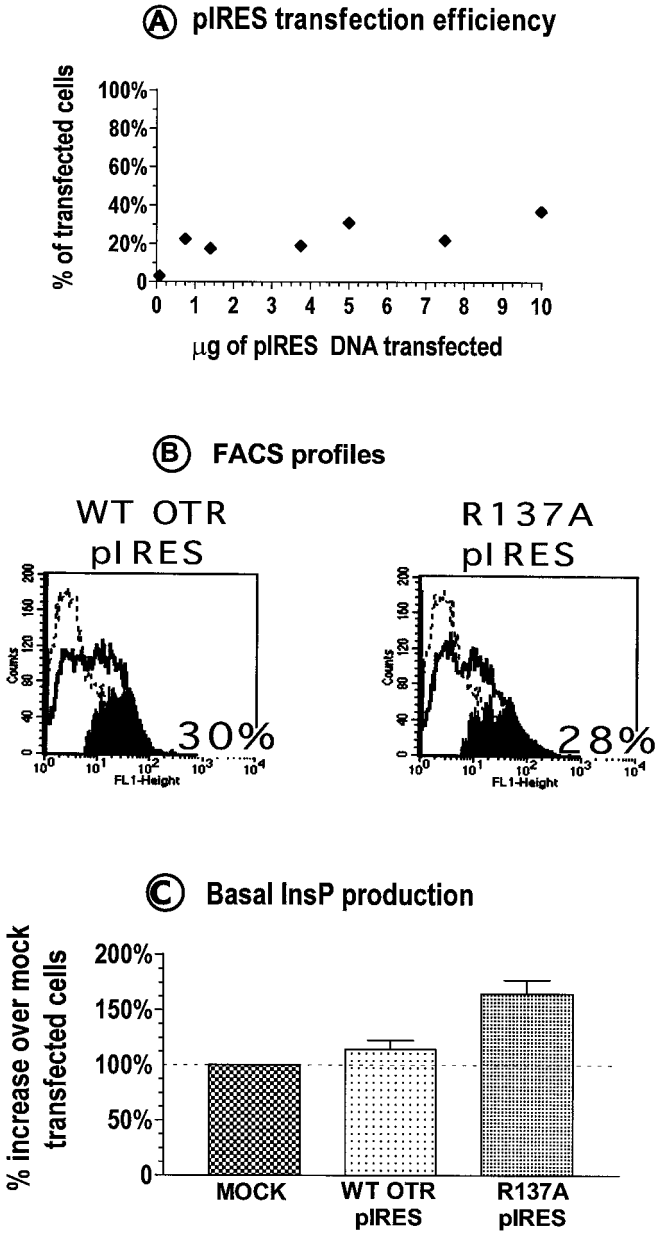

Fig. 3. Evaluation of transfection efficiency. In our experiments, the total DNA transfected (20 μg/electroporation) was maintained constant by adjusting the amount of carrier DNA. A, various amounts of pIRES vector DNA (Clontech) were electroporated into COS7 cells. Percentage of fluorescent transfected cells was determined by FACS analysis. B, FACS profiles of COS7 cells transfected with 0.75 and 7.5 μg of WT-OTR-pIRES and R137A-pIRES DNA. Dotted line represents mock-transfected cells, straight line represents the population of cells electroporated with specific DNA, filled histogram represents fluorescent-transfected cells, the percentage of which is reported on the bottom right. C, basal InsP production of cells transfected with 0.75 and 7.5 μg of WT-OTR-pIRES and R137A-pIRES DNA. In this experiment, performed in triplicate, the basal InsP production of the WT and R137A mutant was expressed as the percentage of increase over that of mock-transfected cells (taken as 100%).

level of receptor expression of the WT and R137A mutant, we performed a set of experiments in which the number of receptors expressed on the cell surface was measured by means of [^{3}H]OT saturation binding on intact cells. In this case, because differences between the desensitization process of the WT and that of the mutant receptor cannot be excluded, the binding assay was performed at 4°C over ice to prevent any ligand-induced endocytosis. Shown in Fig. 5, our data indicate a linear correlation between the increase in cell surface receptors and basal InsP production for both the WT and the R137A mutant OTRs. Even though we were unable to reach very high levels of expression with the R137A mutant, these data confirm that at comparable level of expression, the R137A produced more InsP than the WT receptor.

Binding Properties of Constitutively Active R137A Mutant. Cell homogenates were used to obtain a more detailed pharmacological characterization of the R137A mutant. When assayed with the tritiated agonist [^{3}H]OT, no significant difference in OT affinity between the WT (0.46 ± 0.047 nM; n = 5) and the R137A mutant (1.2 ± 0.81 nM; n = 3) was observed in saturation experiments. Similarly, no changes were found when AVP affinity was measured by means of [^{3}H]OT competitive binding (1.65 ± 0.49 nM; n = 3 and 2.5 ± 0.42 nM; n = 3 for the WT and R137A, respectively). However, the R137A mutant showed a marked reduction (20-fold) in the affinity of the specific cyclic peptidic antagonist OTA, as determined in saturation experiments (0.095 ± 0.033 nM, n = 5; and 1.95 ± 0.81 nM, n = 4 for the WT and R137A, respectively).

We also performed [^{3}H]OT saturation binding experiments in the presence and absence of GTPγS to compare the coupling state of R137A with that of the WT receptor. As shown in Fig. 6, the WT receptor displayed an expected 4-fold increase in the K_D value for OT in the presence of GTPγS, thus indicating that GTPγS is able to uncouple the receptor from the G protein and give rise to a receptor population with lower affinity for OT. On the contrary, in the R137A mutant, no significant change in OT affinity was detected in the presence of GTPγS. These findings support the evidence that the R137A mutant is characterized by (a) particular precoupling state(s) that is/are quite different from that of the WT receptor and that determine(s) its increased basal activity.

Computer Simulation of WT and R137A OTRs. As illustrated in Fig. 7, different interaction patterns involving polar and charged amino acids characterize the average minimized structures of the WT and R137A mutant OTRs.

In the average minimized structure of WT OTR several salt bridge interactions contribute toward stabilizing the receptor "ground state". As shown in Fig. 7, R137 is subjected to the attractive effects of the electrostatic fields generated by the two highly conserved aspartates on helices 2 and 3: D85 and D136, respectively. D136 is also involved in a charge-reinforced H-bonding interaction with R150 (i2). Other charge-reinforced H-bonding interactions constitute structural fea-

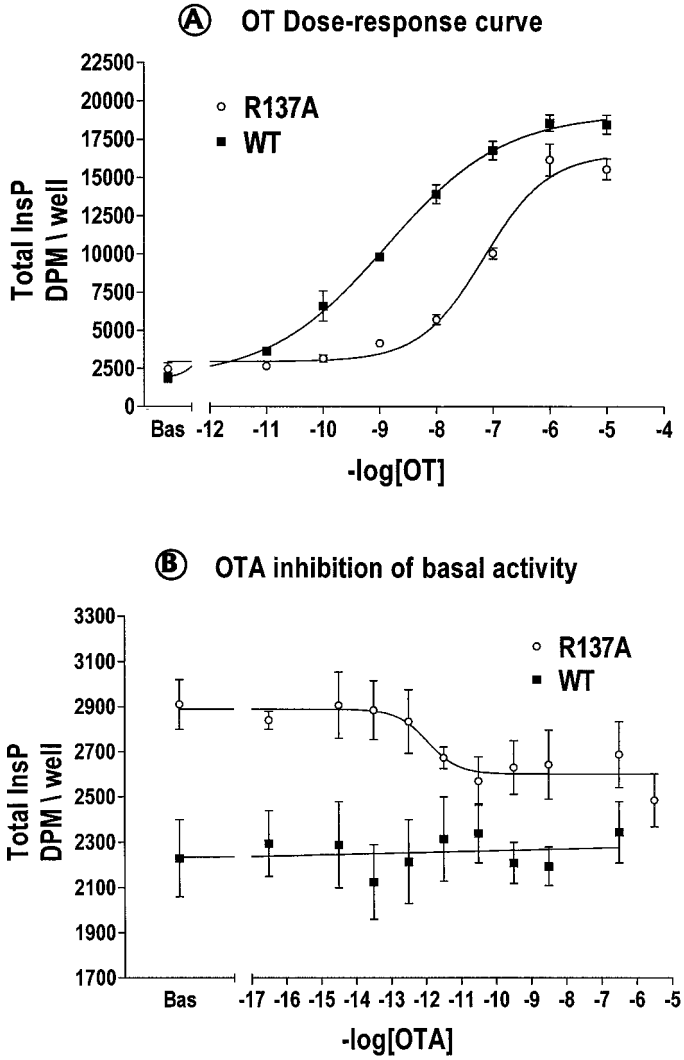

Fig. 4. Agonist and inverse agonist properties of OT and OTA in the WT OTR and R137A mutant. InsP production was measured after the stimulation of transiently transfected COS7 cells with increasing concentrations of peptides. Curves are representative of at least two independent assays performed in triplicate. Each point represents the total amount of InsPs expressed as dpm/well. A, effects of increasing concentrations of OT; in these experiments, we calculated an EC_{50} value of 1.32 ± 0.13 nM and 66.67 ± 1.20 nM for the WT OTR and the R137A mutant, respectively. B, effects of increasing concentrations of the specific antagonist OTA; in this experiment, the IC_{50} value for R137A was 0.1 ± 0.71 pM.

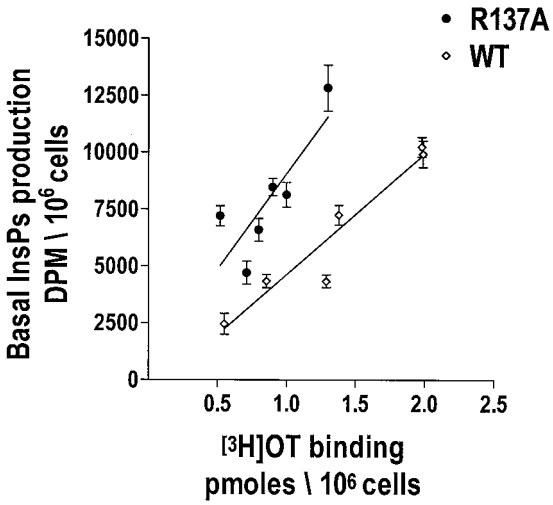

Fig. 5. WT and R137A basal activities as a function of receptor expression levels. WT and R137A receptors were transiently expressed at variable levels in COS7 cells by transfecting increasing amounts of specific plasmid cDNA; basal InsP production and [^{3}H]OT binding were determined as described in *Materials and Methods*. For each transfection, basal InsP production and [^{3}H]OT binding sites were expressed per million of cells present in the well at the time of the determination.

tures of the OTR "ground state". In particular, 1) the D136 (helix 3)/R150 (i2)/D153 (helix 4) interactions produce a structural link between the cytosolic ends of helices 3 and 4; and 2) the R73 (i1)/D251 (i3), the R146 (i2)/E339 (helix 7), and the R149 (i2)/E242 (i3) interactions provide more strength to the intramolecular interactions that connect i1 and i2 with i3 and the cytosolic extension of helix 7. Although these interactions are overemphasized in our structures, which are the results of simulations performed in vacuo, it is conceivable that the attraction between most of these charged residues still operates in the solvated proteins, because these residues should not be separated by a bulk of water molecules. Moreover, the highly conserved amino acids forming a polar pocket near the cytosol, (N57, D85, N325, and Y329) are involved in the following interaction pattern: 1) D85 (helix 2) performs van der Waals attractive interactions with N57 (helix 1) and N325 (helix 7); and 2) N325 (helix 7) and Y329 (helix 7) of the highly conserved NPXXY sequence contribute toward constraining the motion of R137 by means of H-bonding and van der Waals attractive interactions, respectively, with its side chain.

A rearrangement of the interaction patterns involving the "polar pocket" amino acids occurs in the constitutively active R137A mutant structure (Fig. 7). In particular, D85 (helix 2) performs H-bonding interactions with both N57 (helix 1) and N325 (helix 7). Moreover, Y329 is shifted toward helix 2, being directed toward helix 6 in the WT OTR.

The differences in the interaction patterns of the polar pocket amino acids in the WT and R137A mutant are associated with differences in the arrangement of helices and loops (Figs. 7 and 8b). In particular, one of the structural peculiarity of the R137A mutant is the detachment of helices 4 and 5 and the approaching of the cytosolic end of helix 4 to that of helix 2 (Fig. 8a). Moreover, many of the salt bridge interactions, as well as the bulk of the other weaker nonbonding interactions, connecting i1 and i2 with i3 and the cytosolic extension of helix 7 in the WT OTR, are released in the structure of the active mutant (Fig. 7), thus promoting the opening of a solvent accessible site in between i1 and i2, on one hand, and i3, on the other one (Figs. 7 and 8c). In fact, as it can be seen in Fig. 8c, i1 and i2 in the active mutant are characterized by a larger solvent accessible surface than in the WT OTR.

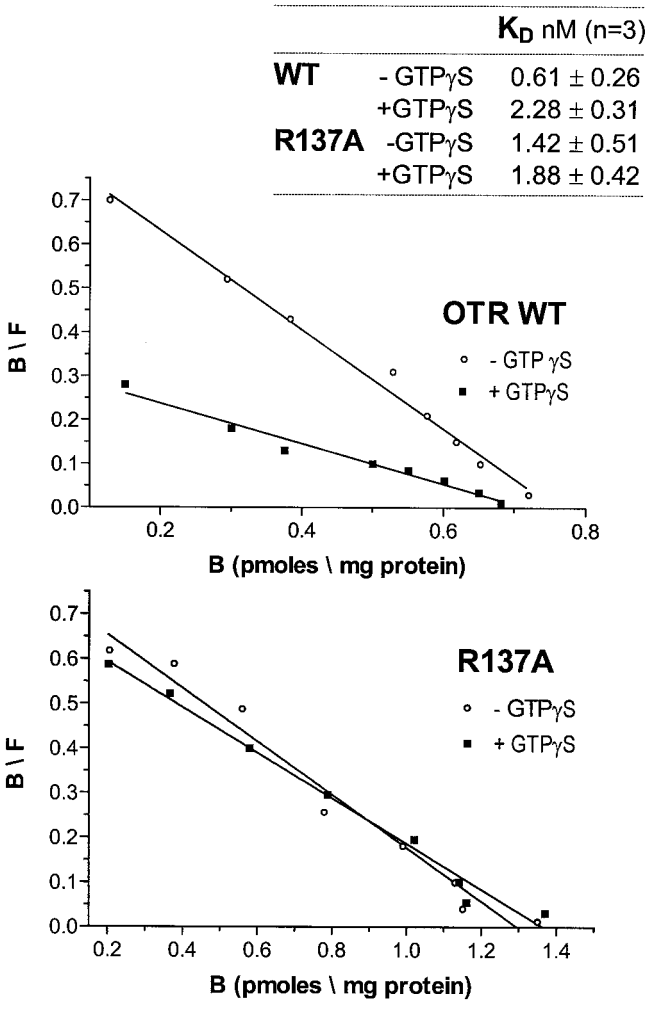

Fig. 6. Effect of GTPγS treatment on [^{3}H]OT affinity in the WT and R137A. Membrane from COS7 cells expressing the WT or the R137A mutant receptors were prepared and preincubated for 10 min in the presence of 100 mM GTPγS; [^{3}H]OT saturation experiments were then performed as described in *Materials and Methods*. Figure shows a Scatchard analysis that is representative of three separate experiments, each performed in triplicate. Mean ± S.E. of the K_D values are shown in the inset.

Computer Simulation of WT and D85A OT/OTR Complexes. To investigate the structural and dynamic features of the agonist-induced active states of OTR, OT was docked into the input structures of the WT OTR and of the agonist-unactivatable D85A mutant.

Among the large number of OT- WT OTR complexes obtained, the average minimized structure showing the best agreement with the experimental data (Fig. 9 and Table 1) was selected for the comparative analysis. However, given the low resolution level of the experimental data available and the consequent absence of any structural constraint, at the atomic level, for choosing the appropriate OT-OTR interaction model, the chosen complex might represent one of the possible models. In this complex, the cyclic part of the peptide (1–6 sequence) docks into the site formed by e2 and the extracellular ends of helices 3, 4, 5, and 6, whereas the linear C-terminal tripeptide (7–9 sequence) mainly docks into the site formed by the amino acid residues of e1, e2, and the extracellular ends of helices 3 and 7 (Figs. 8 and 9). The OT-OTR interaction model presented in this work differs from the previously published model (Chini et al., 1996) as a result of a number of concomitant factors: 1) the arrangement of the seven helices and the conformation of the loops were obtained by means of different methodologies and contain different experimental information, i.e., the present model takes into account the structural information coming from the recently published three-dimensional map of frog rhodopsin (Unger et al., 1997); 2) the input conformation of the hormone is different in the two models; and 3) the amino terminus of the hormone in our model is protonated and not neutral.

The comparison of the free and the OT-bound forms of the WT OTR shows that the agonist induces a structural rearrangement propagating from the extracellular to the intracellular domains (Figs. 7 and 8). In the OT-OTR-simulated complex, the interaction of the hormone with E307 (e3; Fig. 9) induces the breakage of the intramolecular salt bridge found in the free receptor form between K116 (helix 3) and

E307 (e3). The anchoring of the hormone to E307 (e3) by means of the protonated N-terminal nitrogen atom, followed by the interaction with helices 3 and 6, promotes outward motions of the extracellular extensions of the two helices (Fig. 8b). The motion of helix 6 leads to a shift of W288 (helix 6) from the core of the helix bundle (directed toward helix 3) to a position toward helix 5 and the membrane (Fig. 8b). The shift of W288 (helix 6) is consistent with the results of ultraviolet resonance Raman study of the light-induced protein structural changes in rhodopsin activation (Kochendoerfer et al., 1997).

Similar to the R137A active mutant, the OT-bound OTR structure is characterized by the approaching of the cytosolic ends of helices 2 and 4, as compared with WT OTR (Fig. 8b). Another structural peculiarity of the OT-bound OTR structure is the weakening of the attractive effect exerted by both D85 and D136 on R137 in the average structure of the free WT OTR that results into the shift of R143 away from the polar pocket (Fig. 7). Similar to the constitutively active structure R137A, the motions of helices 3, 4, 5, and 6 promote the release of the majority of the salt bridge interactions and of the other weaker interactions connecting i1 and i2 with i3 and the cytosolic extension of helix 7 in the free form of WT OTR (Fig. 7). One consequence of this rearrangement is that i1, i2, i3, and the cytosolic extension of helix 5 become more exposed to the solvent than in the unbound form of WT OTR, as it clearly results from the comparison of their solvent accessible surfaces in the free and the OT-bound forms of WT OTR (Fig. 8c).

The simple substitution of alanine for D85 in the input structure of the OT-OTR complex produces an average arrangement that differs from that of the corresponding complex between OT and the WT receptor. Some of the many structural differences involve the conformation of the hormone (Fig. 9); in fact, the root mean square deviations of the main chain α-carbon atoms of the whole peptide and the cyclic part are, respectively, 1.58 Å and 0.64 Å. Moreover, the interaction patterns involving OT in the complex with the

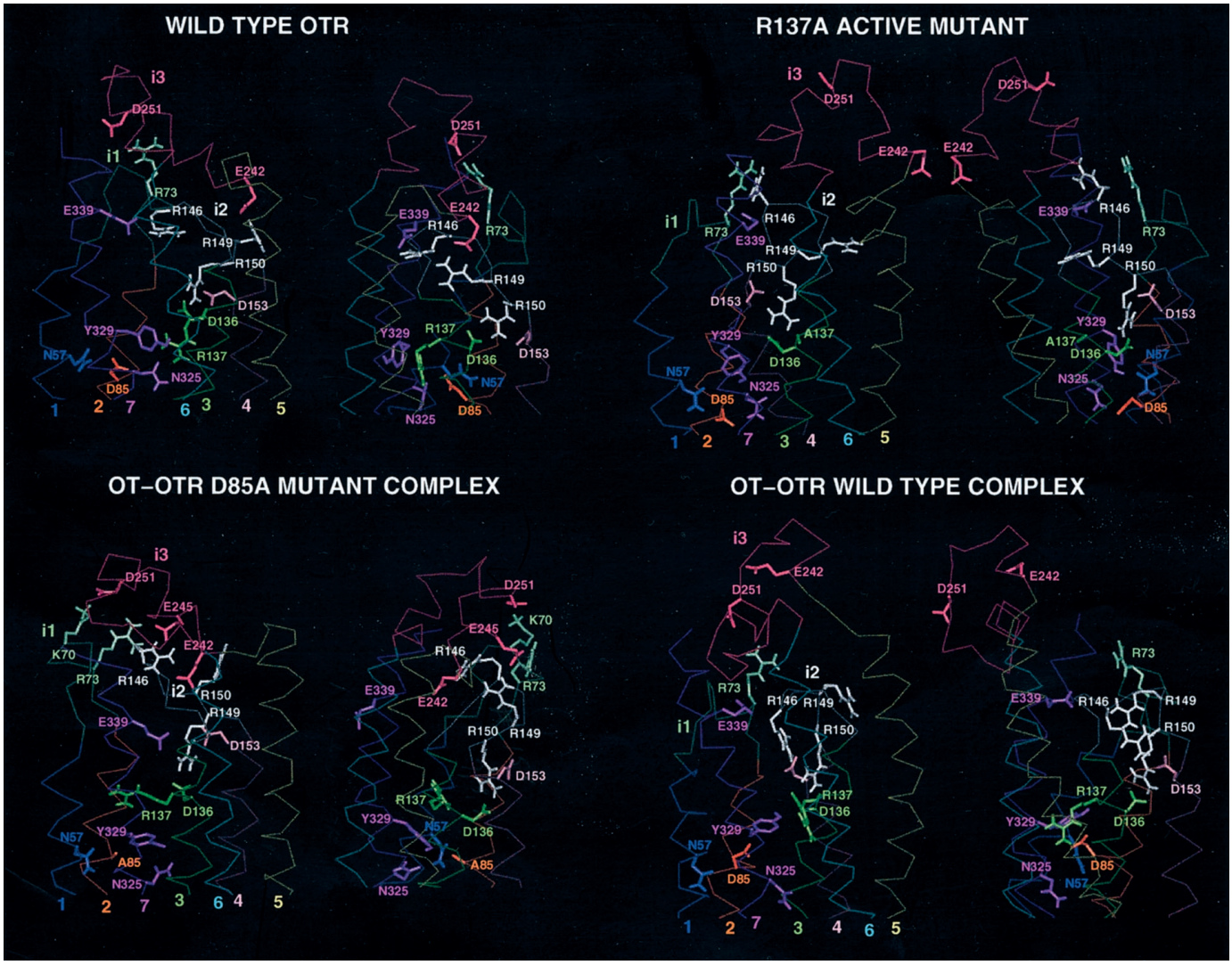

Fig. 7. Average minimized structures of the free and OT-bound forms of WT and mutant OTRs. Intracellular and extracellular sides are at the top and bottom of the helix bundles, respectively. All views are parallel to the membrane surface. The seven helices 1, 2, 3, 4, 5, 6, and 7 are, respectively, colored in blue, orange, green, pink, yellow, sky blue, and violet; i1, i2, and i3 are, respectively, colored in green, white, and rose. The side chains of some amino acids (colored according to their location) located in the environment of D85, D136, and R137 of the E/DRY, as well as of some of the ionic amino acids in the cytosolic loops that contribute to the closing/opening of a cytosolic site in the inactive/active receptor forms, are shown in the figure. Backbone α-carbon atoms of the cytosolic half of the receptor models are also displayed.

D85A mutant differ from those in the corresponding complex with the WT receptor (Table 1 and Fig. 9). One of these differences consists of the lack of the salt bridge interaction between E307 and the protonated N-terminal nitrogen atom of the hormone (Fig. 9). The OT-D85A complex is also characterized by the attractive effect exerted by D136 on R137 that contributes toward constraining the motion of this conserved arginine. One important consequence is that OT is no longer capable of triggering the opening of the solvent-exposed site in the cytosolic domains of the D85A mutant (Figs. 7 and 8c) because i1 and i2 are buried by i3, even more than in the free form of WT OTR (Figs. 7 and 8c).

Discussion

In this study, we analyzed the role of a number of human OTR residues that may be of fundamental importance in the process of receptor activation. By targeting the highly conserved amino acids N57 (helix 1), D85 (helix 2), D136 (helix 3), and R137 (helix 3), we found that mutation of the arginine of the E/DRY sequence into alanine (R137A) leads to a form of the OTR characterized by an increased basal activity. It is worth noting that mutations involving the arginine of the E/DRY sequence in the vasopressin V2 receptor (Rosenthal et al., 1993), as well as in other GPCRs (Zhu et al., 1994; Scheer et al., 1996; Acarya and Karnik; 1996; Arora et al., 1997; Lu et al., 1997), lead to uncoupled receptor forms. However, very recent results of mutagenesis experiments involving the α_{1B}-AR targeting the arginine of the E/DRY sequence have shown that mutations of R143 (corresponding to R137 in OTR) into lysine, histidine, and aspartate induces constitutive activation, whereas mutations into alanine, isoleucine, asparagine, and glutamate lead to a loss of coupling (S.

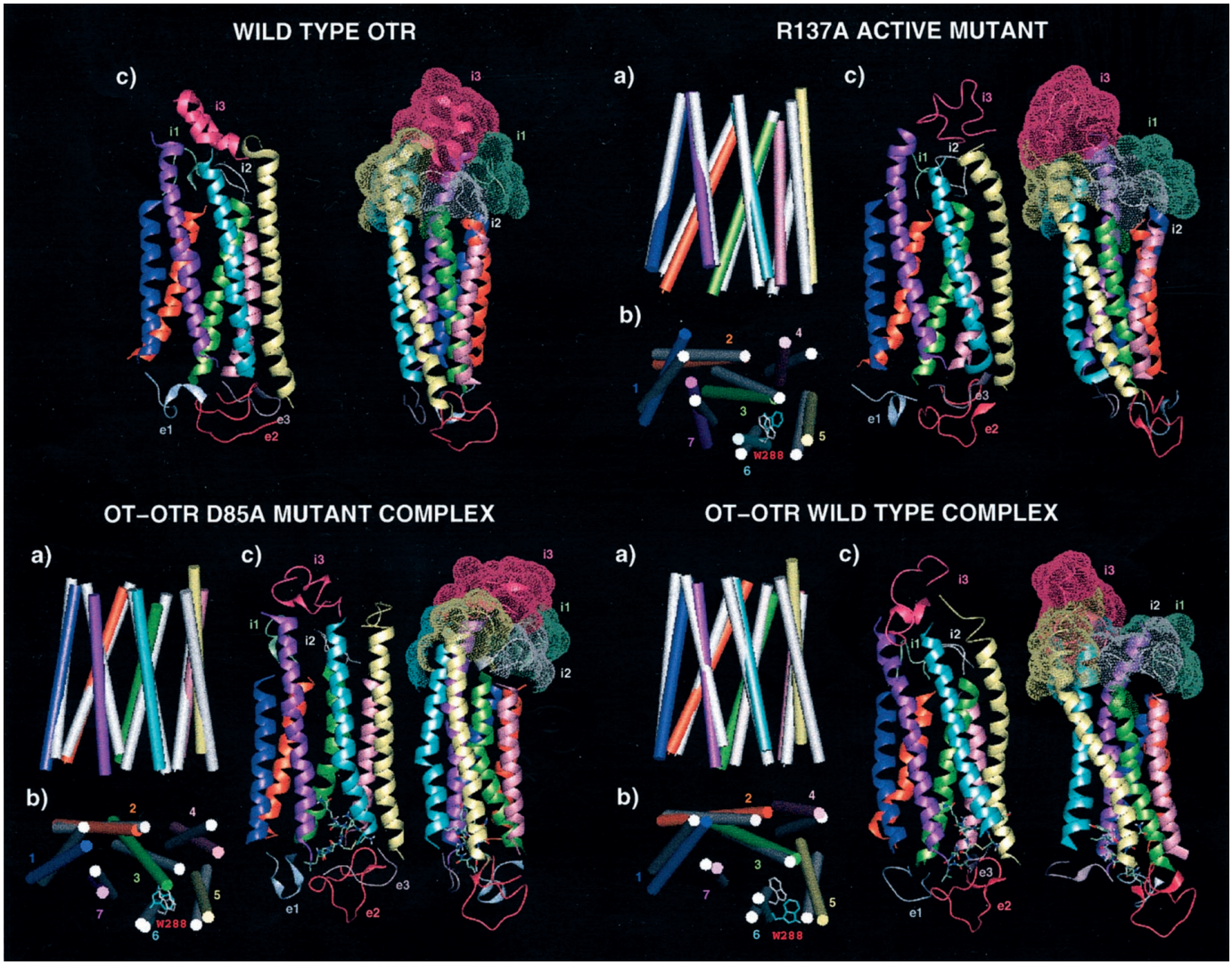

Fig. 8. Average minimized structures of the free and OT-bound forms of WT and mutant OTRs. The intracellular and extracellular sides are at the top and bottom of the helix bundles, respectively. a, cylinder representation of the seven helices of WT OTR superimposed on the structures of the R137A active mutant (top left), the OT-D85A complex (bottom left), and the OT-WT OTR complex (bottom right). Helix bundle is seen in a direction parallel to the membrane surface. WT helices are colored in white, whereas the helices in the other structures are colored as described in Fig. 7. b, cylinder representation like that in point a but seen from the intracellular side in a direction perpendicular to the membrane surface. Side chain of W288 is also displayed. c, two views of the average minimized structure, represented by cartoons. i1, i2, and i3 are, respectively, colored in green, white, and rose, whereas e1, e2, and e3 are, respectively, colored in light blue, red, and carnation. Receptors are seen in a direction parallel to the membrane surface. Solvent-accessible surfaces (represented by dots) computed on i1, i2, i3 and the cytosolic extensions of helices 5 and 6 are shown on the receptor structures in one of the two views. Hormone in the OT-WT OTR and in OT-D85A complexes is represented by liquorices and is colored by atom types.

Cotecchia, personal communication). Similarly, mutations of the arginine of the E/DRY sequence of the β2-AR did not abolish coupling (Seibold et al., 1998). Together these data support the hypothesis that this arginine plays a fundamental role in promoting receptor isomerization into functionally different states.

This hypothesis is consistent with the results of comparative MD simulations of the WT and mutant OTRs. On the basis of these results, R137 should play a fundamental role in constraining the OTR in the ground state, as well as in allowing the transition toward active states. In the WT ground state, the motion of R137 is constrained by the attractive electrostatic field generated by D85 (helix 2) and D136 (helix 3), and by persistent H-bonding interactions with N325 (helix 7). This configuration allows the formation of salt bridges and van der Waals-attractive interactions that keep closed the cytosolic side of the central pore of the helix bundle (Figs. 7 and 8). Mutation R137A triggers rigid body motions that involve the whole helix bundle, leading to the opening of a cytosolic site involving i2, the cytosolic extension of helix 5 and i3 (Fig. 8c). We hypothesize that this cytosolic crevice may play a fundamental role in G protein recognition, consistent with some experimental findings (Wess, 1997).

A change in the interaction pattern of R137 with respect to WT OTR is also one of the structural features of the agonist-induced active state. We found that, to allow the effective transfer of structural information from the extracellular to the intracellular side of the receptor, interactions between the cyclic part of the hormone and the receptor residues on the extracellular ends of helices 3, 5, and 6 needed to be stabilized by the formation of a salt-bridge interaction between the protonated N-terminal amino group of the hormone and E307 (e3) of the receptor (Fig. 9). The establishment of these interactions induces rigid helix body motions that primarily involve helices 3 and 6, and that propagate to the whole helix bundle. As a consequence, the interactions that constrain the motion of R137 and connect i1 and i2 with i3 in the WT "ground state" structure are released, thus promoting the opening of the solvent-exposed site in the cytosolic domains that has been hypothesized to be involved in G protein recognition (Fig. 8c).

The comparative analysis of the average minimized struc-

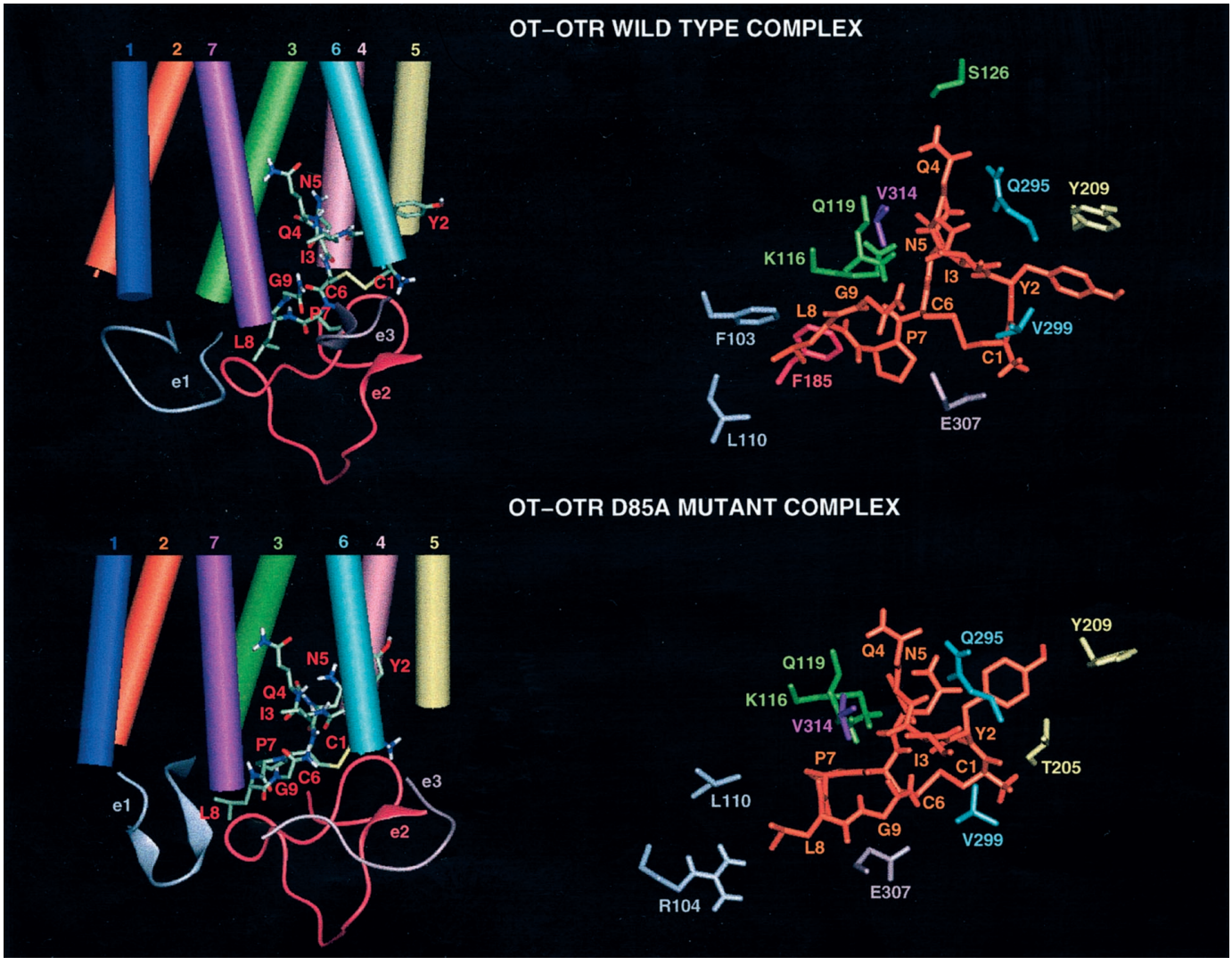

Fig. 9. Agonist binding sites in the OT-bound forms of the WT OTR (top) and the D85A mutant (bottom). Top and bottom left view, docking of the hormone in the extracellular halves of OTRs. Top and bottom right views, details of the interactions of OT with the WT OTR (top) and the D85A mutant (bottom). Color of the side chains of the receptor in the right part of the figure matches that used for the helices and the extracellular regions in the left part. Amino acid residues of the hormone have been also labeled.

tures also suggests that the highly conserved aspartate located on helix 2 has to stay in its deprotonated (anionic form) to allow the rearrangement of the cytosolic domains and the exposure of the G protein docking site to occur. In agreement with this hypothesis, the experimental results show that the D85A mutant is completely uncoupled. Furthermore, computer simulations revealed that the irreversible neutralization of D85 following its mutation into alanine, increases the attractive effect exerted by D136 on R137, thus preventing the agonist-induced structural changes observed in the WT structure (Figs. 7 and 8).

Our results suggest that, although differently triggered, the motion of the helices in the OT-OTR complexes and in the R137A active mutant leads to the opening of a cytosolic crevice in between i2 and i3. However, although the mutation-induced and agonist-induced active forms have a number of structural similarities, there are also some clear differences between them. First, the opening of cytosolic sites, which are formed by the same receptor portions but show slightly different shapes, suggests that different active forms of the same receptor should recognize the G protein with the same domains by establishing different interaction patterns. These differences in receptor/G protein recognition may be responsible for the particular coupling properties of the R137A mutant. Second, several differences between the WT and the R137A active mutant involve the arrangement of the extracellular domains, including the extracellular ends of the helix bundle. These differences in the domains involved in the formation of the agonist binding site should imply a different ability to interact with the agonists. In this respect, it is worth noting that, unlike the great majority of constitutively active receptor mutants, the constitutively active R137A does not show any measurable increase in agonist affinity. Because examples of constitutively active mutants with unchanged affinities for agonists, including a recently identified constitutively active V2 receptor (Morin et al., 1998) have been reported in the literature (Groblewski et al., 1997; Hjorth et al., 1998; Zhao et al., 1998), this property may characterize a subset of constitutively active receptors.

Finally, comparative analysis of the free- and agonist-bound forms of the WT OTR and α_{1B}-AR suggest that the highly conserved polar amino acids and the seven helices should play similar mechanistic roles in the different GPCRs. The ground and inactive states of both receptors are characterized by the constraining effects exerted on the motions of the E/DRY arginine by the conserved aspartates on helices 2 and 3, as well as by the other "polar pocket" amino acids. These effects are weakened in the mutation-induced or agonist-induced active states. Moreover, the helices of both receptors have the fundamental roles of transferring the structural information between the two poles of the helix-bundles and dictating the arrangements of the flexible loops. In the different active forms of both receptors helix motions induce the opening of a solvent-exposed site involving i2, the intracellular extension of helix 5 and i3. Our results showed that, although mutation of the E/DRY arginine into alanine induces opposite structural effects in the OTR and the α_{1B}-AR (Scheer et al., 1996), this fully conserved arginine plays similar mechanistic roles in the agonist-induced activation of these two receptors.

In conclusion, this article reports the first steps in the molecular analysis of the amino acids forming the "polar pocket" of the human OTR and the identification of the first constitutively active mutation of this peptidergic receptor. We proposed a possible docking of the peptide into the receptor that allowed us to describe the similarities and the differences between a mutation-induced and an agonist-induced active state at the molecular level; furthermore, the use of the R137A mutant made it possible to demonstrate that the specific antagonist OTA, one of the most extensively used analogs for characterizing the pharmacological and functional aspects of human OTR, behaves as an inverse agonist. Finally, by comparing the activation process of the OTR with that of the α_{1B}-AR, we found that the receptor domains involved in G protein recognition should be mainly the same in these two members of the rhodopsin family; this finding should allow the planning of future experiments aimed at elucidating the specificity of receptor/G protein recognition.

TABLE 1
Interaction patterns of OT in average minimized complexes of the WT OTR and of D85A mutant

OT	WT OTR	Intermolecular Interaction	D85A	Intermolecular Interaction
C1	T202 (helix 5)	HB[a]	1201 (helix 5)	VDW
C1	V299 (helix 6)	VDW[b]	T205 (helix 5)	HB
C1	W300 (e3)	VDW	W300 (e3)	VDW
C1	E307 (e3)	IONIC HB		
Y2	T205 (helix 5)	VDW	V208 (helix 5)	HB
Y2	L206 (helix 5)	VDW	Y209 (helix 5)	VDW
Y2	Y209 (helix 5)	VDW	F292 (helix 6)	VDW
Y2	M297 (helix 6)	VDW	Q295 (helix 6)	VDW
I3	V294 (helix 6)	VDW	V294 (helix 6)	VDW
I3	V314 (helix 7)	VDW	V314 (helix 7)	VDW
I3	I313 (helix 7)	VDW	I313 (helix 7)	VDW
Q4	M123 (helix 3)	VDW	M123 (helix 3)	VDW
Q4	S126 (helix 3)	HB	F291 (helix 6)	VDW
Q4	Q295 (helix 6)	HB	Q295 (helix 6)	HB
N5	K116 (helix 3)	HB	K116 (helix 3)	HB
N5	M123 (helix 3)	VDW	M123 (helix 3)	VDW
N5	Q171 (helix 4)	HB	Q171 (helix 4)	VDW
N5			I174 (helix 4)	VDW
N5			V208 (helix 5)	VDW
C6	Q119 (helix 3)	HB	E307 (e3)	VDW
P7	E307 (e3)	VDW	R113 (helix 3)	VDW
P7			Q119 (helix 3)	VDW
L8	F103 (e1)	VDW	F103 (e1)	VDW
L8	L110 (e1)	VDW	R104 (e1)	VDW
L8	V115 (helix 3)	VDW	L110 (e1)	VDW
L8	F185 (e2)	VDW	A310 (helix 7)	VDW
L8	V184 (e2)	VDW		
G9	A310 (helix 7)	VDW	V299 (helix 6)	VDW

[a] HB, hydrogen bonding interaction.
[b] VDW, van der Waals attractive interaction.

Acknowledgments

We are indebted to C. Barberis and M. Manning for proving us with the labeled and unlabeled OTA antagonist, to T. Kimura for the gift of the human OTR cDNA, and to S. Cotecchia and D. Fesce for critically reading the manuscript. We are grateful to S. Saini for technical help, to Centro Interdipartimentale di Calcolo Automatico ed Informatica Applicata (University of Modena) for technical help and for allowing us to use its computer facilities, to S. Citterio and M. Rescigno for help with FACS analysis.

References

Acharya S and Karnik SS (1996) Modulation of GDP release from transducin by the conserved Glu134-Arg135 sequence in rhodopsin. *J Biol Chem* **269:**25406–25411.
Arora KK, Cheng Z and Catt KJ (1997) Mutations of the conserved DRS motif in the second intracellular loop of the gonadotropin-releasing hormone receptor affect expression, activation, and internalization. *Mol Endocrinol* **11:**1203–1212.
Baldwin JM, Schertler GF and Unger VM (1997) An alpha-carbon template for the

transmembrane helices in the rhodopsin family of G-protein-coupled receptors. *J Mol Biol* **272:**144–164.
Brooks BR, Bruccoleri RE, Olafson BD, States DJ, Swaminathan S and Karplus M (1983) CHARMM: A program for macromolecular energy minimization and dynamics calculations. *J Comput Chem* **4:**187–217.
Chini B, Mouillac B, Ala Y, Balestre M, Trumpp-Kallmeyer S, Hoflack J, Elands J, Hibert M, Manning M, Jard S and Barberis C (1995) Tyr115 is the key residue for determining receptor selectivity in the V1a vasopressin receptor. *EMBO J* **14:** 2176–2182.
Chini B, Mouillac B, Balestre M, Trumpp-Kallmeyer S, Hoflack J, Hibert M, Andriolo M, Pupier S, Jard S and Barberis C (1996) Two aromatic residues regulate the response of the human oxytocin receptor to the partial agonist arginine vasopressin. *FEBS Lett* **397:**201–206.
Coleman, DE and Sprang, S (1996) How G-proteins work: A continuing story. *Trends Pharmacol Sci* **21:**41–44.
Cotecchia S, Exum S, Caron MG and Lefkowitz RJ (1990) Regions of the α1-adrenergic receptor involved in coupling to phosphatidylinositol hydrolysis and enhanced sensitivity of biological function. *Proc Natl Acad Sci USA* **87:**2896–2900.
Elands J, Barberis C, Jard S, Tribollet E, Dreifuss J, Bankowski K, Manning M and Sawyer WH (1987) 125I-labelled d(CH_2)$_5$[Tyr(Me)^2, Thr^4, Tyr-NH_2^{9}]OVT: A selective oxytocin receptor ligand. *Eur J Pharmacol* **147:**197–207.
Fanelli F, Menziani C, Scheer A, Cotecchia S and De Benedetti PG (1998) Ab initio modeling and molecular dynamics simulation of the α1b-adrenergic receptor activation. *Methods (Orlando)* **14:**302–317.
Farrens DL, Altenbach C, Yang K, Hubbell WL and Khorana HG (1996) Requirement of rigid-body motion of transmembrane helices for light activation of rhodopsin. *Science (Wash DC)* **274:**768–770.
Franzoni L, Nicastro G, Pertinhez TA, Tatò M, Nakaie CR, Paiva ACM, Schreier S and Spisni A (1997) Structure of the C-terminal fragment 300–320 of the rat angiotensin II AT1A receptor and its relevance with respect to G-protein coupling. *J Biol Chem* **272:**9734–9741.
Gether U, Lin S, Ghanouni P, Ballesteros JA, Weinstein H and Kobilka BK (1997) Agonist induces conformational changes in transmembrane domains III and VI of the β2-adrenoceptor. *EMBO J* **16:**6737–6747.
Groblewski T, Maigret B, Larguier R, Lombard C, Bonnafous JC and Marie J (1997) Mutation of ASN111 in the third transmembrane domain of the AT1A angiotensin II receptor induces its constitutive activation. *J Biol Chem* **272:**1822–1826.
Hjorth SA, Orskov C and Schwartz TW (1998) Constitutive activity of glucagon receptor mutants. *Mol Endocrinol* **12:**78–86.
Jung H, Windhaber R, Palm D and Schnackerz K (1995) NMR and circular dichroism studies of synthetic peptides derived from the third intracellular loop of the β-adrenoreceptor. *FEBS Lett.* **358:**133–136.
Jung H, Windhaber R, Palm D and Schnackerz K (1996) Conformation of a β-adrenoceptor-derived signal transduction peptide as inferred by Circular Dichroism and 1H NMR spectroscopy. *Biochemistry* **35:**6399–6405.
Kochendoerfer GG, Kaminaka S and Mathies R (1997) Ultraviolect resonance raman examination of the light-induced protein structural changes in rhodopsin activation. *Biochemistry* **36:**13153–13159.
Kojro E, Eich P, Gimpl G and Fahrenholz (1993) Direct identification of an extracellular agonist binding site in the renal V2 vasopressin receptor. *Biochemistry* **32:**13537–13544.
Liu J and Wess J (1996) Different single receptor domains determine the distinct G-protein coupling profiles of members of the vasopressin receptor family. *J Biol Chem* **271:**8772–8778.
Lu ZL, Curtis CA, Jones PG, Pavia J and Hulme EC (1997) The role of the aspartate-arginine-tyrosine triad in the m1 muscarinic receptor—mutations of aspartate 122 and tyrosine 124 decrease receptor expression but do not abolish signaling. *Mol Pharmacol* **51:**234–241.
Morin D, Cotte N, Balestre MN, Mouillac B, Manning M, Breton C and Barberis C (1998) The D136A mutation of the V2 vasopressin receptor induces a constitutive activity which permits discrimination between antagonists with partial agonist and inverse agonist activities. *FEBS Lett* **441:**470–475.
Mouillac B, Chini B, Balestre MN, Elands J, Trumpp-Kallmeyer S, Hoflack J, Hibert M, Jard S and Barberis C (1995) The binding site of neuropeptide vasopressin V1a receptor: Evidences for a major localization within transmembrane regions. *J Biol Chem* **270:**25771–25777.
Munson PJ and Rodbard, D (1980) Ligand: A versatile computerized approach for characterization of ligand binding systems. *Anal Biochem* **107:**220–239.
Pellegrini M, Royo M, Chorev M and Mierke DF (1996) Conformational characterisation of a peptide mimetic of the third cytoplasmic loop of the G-protein coupled parathyroid hormone/parathyroid hormone related protein receptor. *Biopolymers* **40:**643–666.
Postina R, Kojro E and Fahrenholz F (1996) Separate agonist and peptide antagonist binding sites of the oxytocin receptor defined by their tranfer into the V2 vasopressin receptor. *J Biol Chem* **271:**31593–31601.
Rose JP, Wu CK, Hsiao CD, Breslow E and Wang BC (1996) Crystal structure of the meurophysin-oxytocin complex. *Nature Struct Biol* **3:**163–169.
Rosenthal W, Antaramiam A, Gilbert S and Birnbaumer M (1993) Nephrogenic diabetes insipidus. A V2 vasopressin receptor unable to stimulate adenylyl cyclase. *J Biol Chem* **268:**13030–13033.
Rost B, Fariselli O and Casadio R (1996) Topology predictions for helical transmembrane proteins at 86% accuracy. *Protein Sci* **5:**1705–1718.
Sali A and Blundell TL (1993) Comparative protein modeling by satisfaction of spatial restraints. *J Mol Biol* **234:**779–815.
Samama P, Cotecchia S, Costa T and Lefkowitz RJ (1993) A mutation-induced activated state of the β2-adrenergic receptor. Extending the ternary complex model. *J Biol Chem* **268:**4625–4636.
Scheer A, Fanelli F, Costa T, De Benedetti PG and Cotecchia S (1996) Constitutively active mutants of the α1B-adrenergic receptor: Role of highly conserved polar amino acids in receptor activation. *EMBO J* **15:**3566–3578.
Scheer A, Fanelli F, Costa T, De Benedetti PG and Cotecchia S (1997) The activation process of the α1B-adrenergic receptor: Potential role of protonation and hydrophobicity of a highly conserved aspartate. *Proc Natl Acad Sci USA* **94:**808–813.
Seibold DG, Dagarag M and Birnbaumer M (1998) Mutations of the DRY motif that preserve beta-2-adrenoceptor coupling. *Recept Chan* **5:**375–385.
Unger VM, Hargrave PA, Baldwin JM and Schertler GF (1997) Arrangement of rhodopsin transmembrane alpha-helices. *Nature (Lond)* **389:**203–206.
Wess J (1997) G-protein-coupled receptors: Molecular mechanisms involved in receptor activation and selectivity of G-protein recognition. *FASEB J* **11:**346–354.
Woods SP, Tickle IJ, Trearne AM, Pitts JE, Mascarenhas Y, Li JY, Huscin J, Cooper S, Blundell TL, Hruby VJ and Baku A (1986) Crystal structure analysis of deamino-oxytocin: Conformational flexibility and receptor binding. *Science (Wash DC)* **232:**633–636.
Yeagle PL, Aldeefer JL and Albert AD (1997) Three-Dimensional structure of the cytoplasmic face of the G-protein receptor rhodopsin. *Biochemistry* **36:**9649–9654.
Zhao MM, Gaivin RJ and Perez DM (1998) The third extracellular loop of the β2-adrenergic receptor can modulate receptor/G protein affinity. *Mol Pharmacol* **53:**524–529.
Zhu SZ, Wang SZ, Hu JR and Elfakahany EE (1994) An arginine residue conserved in most G-protein coupled receptors is essential for the function of the m1 muscarinic receptor. *Mol Pharmacol* **45:**517–523.

Send reprint requests to: Dr. Bice Chini, Consiglio Nazionale delle Richerche Cellular and Molecular Pharmacology Center, via Vanvitelli 32, 20129 Milan, Italy. E-mail: Bice@Farma10.csfic.mi.cnr.it